AGU PUBLICATIONS

Earth's Future

RESEARCH ARTICLE

10.1002/2016EF000505

Extreme sea levels on the rise along Europe's coasts

Michalis I. Vousdoukas[1,2], Lorenzo Mentaschi[1], Evangelos Voukouvalas[1], Martin Verlaan[3], and Luc Feyen[1]

[1]European Commission, Joint European Research Centre (JRC), Ispra, Italy , [2]Department of Marine Sciences, University of the Aegean, Mitilene, Greece, [3]Deltares, Delft, The Netherlands

Key Points:
- Projections of ESL including mean sea level, tides, waves and storm surges until 2100, in view of RCP4.5 and RCP8.5, for Europe
- One hundred-year ESL on average projected to increase by 57 cm for RCP4.5 and 81 cm for RCP8.5
- By the end of this century, 5 million Europeans currently under threat of a 100-year ESL could be annually at risk from coastal flooding

Corresponding author:
M. I. Vousdoukas,
Michail.VOUSDOUKAS@ec.europa.eu

Citation:
Vousdoukas, M. I., L. Mentaschi, E. Voukouvalas, M. Verlaan, and L. Feyen (2017), Extreme sea levels on the rise along Europe's coasts, *Earth's Future*, *5*, 304–323, doi:10.1002/2016EF000505.

Received 19 NOV 2016
Accepted 30 JAN 2017
Published online 13 MAR 2017

Abstract Future extreme sea levels (ESLs) and flood risk along European coasts will be strongly impacted by global warming. Yet, comprehensive projections of ESL that include mean sea level (MSL), tides, waves, and storm surges do not exist. Here, we show changes in all components of ESLs until 2100 in view of climate change. We find that by the end of this century, the 100-year ESL along Europe's coastlines is on average projected to increase by 57 cm for Representative Concentration Pathways (RCP)4.5 and 81 cm for RCP8.5. The North Sea region is projected to face the highest increase in ESLs, amounting to nearly 1 m under RCP8.5 by 2100, followed by the Baltic Sea and Atlantic coasts of the UK and Ireland. Relative sea level rise (RSLR) is shown to be the main driver of the projected rise in ESL, with increasing dominance toward the end of the century and for the high-concentration pathway. Changes in storm surges and waves enhance the effects of RSLR along the majority of northern European coasts, locally with contributions up to 40%. In southern Europe, episodic extreme events tend to stay stable, except along the Portuguese coast and the Gulf of Cadiz where reductions in surge and wave extremes offset RSLR by 20–30%. By the end of this century, 5 million Europeans currently under threat of a 100-year ESL could be annually at risk from coastal flooding under high-end warming. The presented dataset is available through this link: http://data.jrc.ec.europa.eu/collection/LISCOAST.

Plain Language Summary Future extreme sea levels and flood risk along European coasts will be strongly impacted by global warming. Here, we show changes in all acting components, i.e., sea level rise, tides, waves, and storm surges, until 2100 in view of climate change. We find that by the end of this century the 100-year event along Europe will on average increase between 57 and 81 cm. The North Sea region is projected to face the highest increase, amounting to nearly 1 m under a high emission scenario by 2100, followed by the Baltic Sea and Atlantic coasts of the UK and Ireland. Sea level rise is the main driver of the changes, but intensified climate extremes along most of northern Europe can have significant local effects. Little changes in climate extremes are shown along southern Europe, with the exception of a projected decrease along the Portuguese coast and the Gulf of Cadiz, offseting sea level rise by 20–30%. By the end of this century, 5 million Europeans currently under threat of a 100-year coastal flood event could be annually at risk from coastal flooding under high-end warming.

1. Introduction

Climate change adaptation and disaster risk reduction have been recognized as a priority worldwide, exemplified by global frameworks such as the Paris Agreement [*United Nations Framework Convention on Climate Change*, 2015] and the Sendai Framework for Disaster Risk Reduction [*United Nations Office for Disaster Risk Reduction*, 2015], and European actions like the EU Climate Change Adaptation Strategy [*European Commission*, 2013] and the Floods Directive [*European Commission*, 2007]. It has been highlighted that reliable risk assessments are essential to take effective disaster risk reduction and adaptation actions [*Mechler et al.*, 2014; *Cutter and Gall*, 2015]. A particular threat that may emerge as a consequence of climate change is the increase in coastal flood risk [*Intergovermental Panel on Climate Change*, 2014]. Coastal flooding is driven by ESLs, being the result of several components, namely the mean sea level (MSL), astronomical tide and episodic water level fluctuations due to climate extremes (waves and storm surges).

Being an alarming phenomenon, sea level rise (SLR) has gained the attention of scientists, who have reported historical [*Chen et al.*, 2014; *Dangendorf et al.*, 2014; *Jevrejeva et al.*, 2014] and future trends [*Pardaens et al.*, 2011; *Kopp et al.*, 2014; *Slangen et al.*, 2014; *Little et al.*, 2015; *Carson et al.*, 2016; *Mengel et al.*,

2016]. This will lead to increased coastal impacts in Europe [*Hinkel et al.*, 2010] and worldwide [*Hauer et al.*, 2016; *Hinkel et al.*, 2014]. Coastal impact assessments to date typically focused solely on SLR, considering stationary contributions from tides, waves and storm surges [*Hinkel et al.*, 2010, 2014; *Brown et al.*, 2013; *Hauer et al.*, 2016]. However, most coastal impacts related to extreme sea levels (ESLs) when waves and surges transfer considerable amounts of energy towards the coast, driving morphological changes and erosion [*Ciavola et al.*, 2011], as well as coastal protection failure [*Oumeraci*, 1994] and overwash/inundation [*Matias et al.*, 2008; *McCall et al.*, 2010]. Novel projections show that changing climate may affect waves [*Hemer et al.*, 2013; *Semedo et al.*, 2013; *Wang et al.*, 2014], storm surges [*Lowe and Gregory*, 2005; *Meier*, 2006; *Woth et al.*, 2006; *Debernard and Røed*, 2008; *Lowe et al.*, 2009; *Weisse et al.*, 2009; *Brown et al.*, 2010; *Marcos et al.*, 2011; *Brown et al.*, 2012; *Gräwe and Burchard*, 2012; *Marcos et al.*, 2012; *Jordà et al.*, 2012; *Conte and Lionello*, 2013; *Gaslikova et al.*, 2013; *Howard et al.*, 2014; *Androulidakis et al.*, 2015; *Vousdoukas et al.*, 2016a], and tides [*Pickering et al.*, 2012; *Pelling and Mattias Green*, 2014; *Arns et al.*, 2015]. Some regional studies even suggest that intensifying climate extremes could dominate SLR in terms of capacity to drive increasing coastal flooding [*Ruggiero*, 2013].

Despite these important advances, no coherent projections of ESLs exist along the European coastline. While the aforementioned regional studies are characterized by differences in the spatial coverage, scenarios, and the methodology, impeding to draw universal conclusions. The present contribution aims to filling this knowledge gap by, for the first time, combining dynamic simulations of all the major components of ESL, considering the latest CMIP5 projections for Representative Concentration Pathways (RCP)4.5 and RCP8.5. As a metric of potential impacts, we focus on changes in the magnitude and frequency of occurrence of the present 100-year ESL (ESL_{100}). The authors are confident that the results of the study, including a public-access dataset of ESL (available from this URL: http://data.jrc.ec.europa.eu/collection/LISCOAST), can be beneficial for research and policy-making efforts toward the timely response to climate impacts along European coasts.

2. Methods

2.1. General Definitions

ESL are driven by the combined effect of MSL, tides (η_{tide}) and water level fluctuations due to waves and storm surges (η_{w-ss}). As a result, ESL can be defined as:

$$ESL = MSL + \eta_{tide} + \eta_{w-ss} \quad (1)$$

The climate extremes contribution η_{w-ss} from waves and storm surge was estimated according to the following equation:

$$\eta_{w-ss} = SSL + 0.2 \times H_s \quad (2)$$

where SSL is the storm surge level, H_s is the significant wave height and $0.2 \times H_s$ is a generic approximation of the wave setup [*U.S. Army Corps of Engineers*, 2002]. Wave setup up is an episodic wave-driven increase in mean water level near the coast, resulting from wave shoaling and breaking processes [*Bowen et al.*, 1968].

The present work has focused on a baseline "historical" period and two climate change scenarios expressed by the RCPs defined by the fifth Assessment Report (AR5) of Intergovermental Panel on Climate Change: RCP4.5 and RCP8.5 [*Meinshausen et al.*, 2011]. RCPs are named after a possible range of radiative forcing values in the year 2100 relative to pre-industrial values (+2.6, +4.5, +6.0, and +8.5 W/m^2, respectively). RCP4.5 and RCP8.5 scenario correspond to a likely global mean temperature increase of 2.0–3.6°C and 3.2–5.4°C in 2081–2100 above the 1850–1900 levels [*Intergovermental Panel on Climate Change*, 2013], respectively. RCP4.5 may be viewed as a moderate-emission-mitigation-policy scenario, and RCP8.5 as a high-end, business-as-usual scenario.

2.2. Projections of RSLR

Projections of SLR for RCP2.5 and RCP8.5 were available from Hinkel et al. [2014], who combined SLR projections from thermal expansions from four global climate models (GCMs), with estimated contributions from ice-sheets and glaciers [for more info; see *Hinkel et al.*, 2014]. Global relative sea level rise (RSLR) values for different RCPs and time slices were produced after combining SLR with land uplift/subsidence projections

from Peltier [2004]. Given that the SLR dataset is the result of a four-member GCM ensemble and for each GCM three ice-sheet and glacier contributions exist, the best, worst, and ensemble mean RSLR cases were estimated for each RCP.

2.3. Projections of Tidal Elevation

Present-state tidal elevations (η_{tide}) along the European coastline were obtained from the TOPEX/POSEIDON Global Inverse Solution [*Egbert and Erofeeva*, 2002]. Given that the focus is on extreme events, the maximum tide (η_{tide}^{max}) was considered as representative. In order to assess how changing sea levels affect tidal elevations, dynamic simulations of tidally forced ocean circulation were performed for each RSLR scenario using a flexible mesh setup of the DFLOW FM model that was extensively validated [*Jagers et al.*, 2014; *Muis et al.*, 2016]. All simulations covered the period from 1990 to 2110 and considered the six possible RSLR scenarios resulting from the combination of the best, worst, and ensemble mean cases for each of the two RCPs.

Maximum tides were estimated from the hourly time series of tidal elevation for the baseline ($\eta_{tide,RCP_{baseline}}^{max}$) and future times slices ($\eta_{tide,RCP_{future}}^{max}$). The TOPEX/POSEIDON baseline values were then combined with the projected relative changes to obtain the final projections:

$$\eta_{tide,RCP}^{max} = \eta_{tide,TOPEX}^{max} + \eta_{tide,TOPEX}^{max} \times \left(\frac{\eta_{tide,RCP_{baseline}}^{max} - \eta_{tide,RCP_{future}}^{max}}{\eta_{tide,RCP_{baseline}}^{max}} \right) \quad (3)$$

2.4. Projections of Climate Extremes

2.4.1. GCMs

Projections of waves and storm surges were based on hydrodynamic simulations with Delft3D-FLOW and WW3 driven by atmospheric forcing from six Coupled Model Intercomparison Project Phase 5 (CMIP5) climate models for both RCP trajectories: ACCESS1.0, ACCESS1.3 (CSIRO-BOM), CSIRO-Mk3.6.0 (CSIRO-QCCCE Australia), EC-EARTH (EC-EARTH consortium), GFDL-ESM2G, and GFDL-ESM2M (NOAA Geophysical Fluid Dynamics Laboratory, USA). Climate model uncertainties were reduced to the greatest possible extent by (1) selecting the CMIP5 climate models that according to Perez et al. [2014] are ranked with high skill in reproducing the synoptic climatologies and inter-annual variations across Europe; and (2) using a validated reanalysis, based on detailed atmospheric forcing, to correct for bias in the wave and storm surge projections generated from each GCM [*Vousdoukas et al.*, 2016a].

2.4.2. Storm Surges

The storm surge contribution to the ESL was estimated using Delft3D-FLOW. The model was validated by comparing hindcast surge simulations from 1979 to 2014 forced by atmospheric pressure and wind fields from the ERA-Interim database against water level time series available from the JRC Sea Level Database (http://webcritech.jrc.ec.europa.eu/SeaLevelsDb). The surge dataset, as well as a detailed description of the model setup, calibration, and validation are available [*Vousdoukas et al.*, 2016a]. For the present study, the storm surge time series for all studied time periods and RCPs were considered, combined with the wave projections (see Section 2.4.2).

2.4.3. Waves

Projections of wave generation/propagation were obtained using the third generation spectral wave model Wavewatch III (WW3) [*Tolman*, 2002] in combination with the last generation growth/dissipation source terms [*Ardhuin et al.*, 2010]. These source terms, based on *Bidlot et al.* [2007], introduce a term for the dissipation of the long swell as a function of the wind, improving the description of the evolution of waves on long distances, with a positive impact on the model performance on global scale [*Ardhuin et al.*, 2010; *Rascle and Ardhuin*, 2013].

The simulations took place on a global 1.5° grid, combined with several nested finer sub-grids on the following specific areas (see Figure 1): (1) Northern Europe (resolution: 0.25°); (2) Mediterranean Sea (resolution: 0.25°); (3) South Western Europe (resolution: 0.5°); (4) Red Sea and Persian Gulf (resolution: 0.25°); (5) Sea of Japan, Eastern Chinese Sea and Sea of Okhotsk (resolution: 0.33°); (6) Hudson bay, (resolution: 0.25°); (7) Gulf of Mexico, (resolution: 0.33°), and (8) South Western Pacific (resolution: 0.5°);.

The model was validated on the grounds of the skill of a reanalysis covering 35 years between 1980 and 2014, forced by ERA-Interim wind data. Modeled wave heights were compared with altimeter data provided

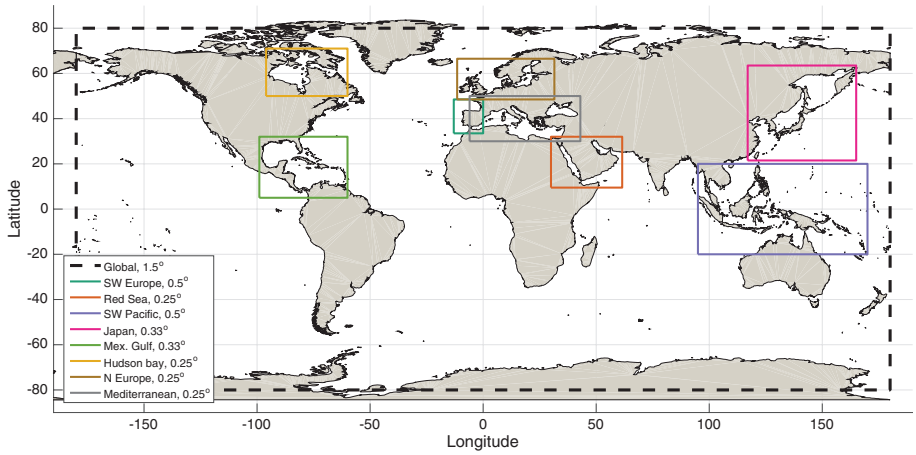

Figure 1. Wave model setup: world map showing the nine nested grids used for the global wave generation/propagation simulations.

by 6 different satellites [*Queffeulou and Croizé-Fillon*, 2014]: ERS-2, ENVISAT, Jason 1 and 2, Cryosat 2, and SARAL-AltiKa. A further validation was carried out using the measurements provided by buoys located mainly in Europe and America. All validation efforts using both datasets can be found in the Appendix A and results were considered satisfactory.

2.4.4. Non-Stationary Extreme Value Statistics

Waves and storm surges were combined into η_{w-ss} time series obtained according to equation (2), and to which non-stationary extreme value statistical analysis (EVA) was applied [*Mentaschi et al.*, 2016]. The statistical analysis consisted in (1) applying a time-varying normalization to transform the non-stationary time series into a stationary one, to which the stationary EVA theory was applied; and (2) reverse-transforming the result into a non-stationary extreme value distribution. From the latter η_{w-ss} values for different return periods were derived for the baseline and during the present century, with a specific focus on the 1 in 100-year event. Links to the source code and a detailed description of the non-stationary EVA approach can be found in *Mentaschi et al.* [2016].

2.5. Relative Changes and Statistical Model Agreement

Projected values of ESL and its components were estimated for the different climate ensemble members. Ensemble mean values represent the most likely case, whereas the ensemble minima and maxima are considered as the best and worst case scenarios and provide an indication of the climate related spread.

The coefficient of variation CV [*Alfieri et al.*, 2015] was used to express the uncertainty introduced by the GCM ensemble:

$$\mathrm{CV} = \frac{\sigma_{\Delta\mathrm{ESL}}}{\Delta\mathrm{ESL}} \tag{4}$$

with $\Delta\mathrm{ESL} = \mathrm{ESL}_{\mathrm{RCP}} - \mathrm{ESL}_{\mathrm{baseline}}$ the absolute change in ESL between the future and baseline period, and $\sigma_{\Delta\mathrm{ESL}}$ the standard deviation of the ΔESL values produced by the six-member GCM ensemble. In addition, relative changes were obtained through normalizing ΔESL by dividing with the baseline values:

$$N\Delta\mathrm{ESL} = 100 \times \frac{\mathrm{ESL}_{\mathrm{RCP}} - \mathrm{ESL}_{\mathrm{baseline}}}{\mathrm{ESL}_{\mathrm{baseline}}} \tag{5}$$

For $|\mathrm{CV}| > 1$ changes were not considered, which roughly corresponds to an average agreement of five out of six models (i.e., 84% probability) when assuming that relative changes are normally distributed [*Alfieri et al.*, 2015]. The percentage of change in ESL that can be attributed to changes in extremes of waves and storm surges was estimated as follows:

$$\%\Delta\eta_{w-ss} = 100 \times \frac{\Delta\eta_{w-ss}}{\mathrm{RSLR}} \tag{6}$$

While the CV indicates agreement between the GCMs, Mann–Kendall tests were used to assess whether the projected changes from the ensemble mean were statistically significant [*Kendall*, 1975].

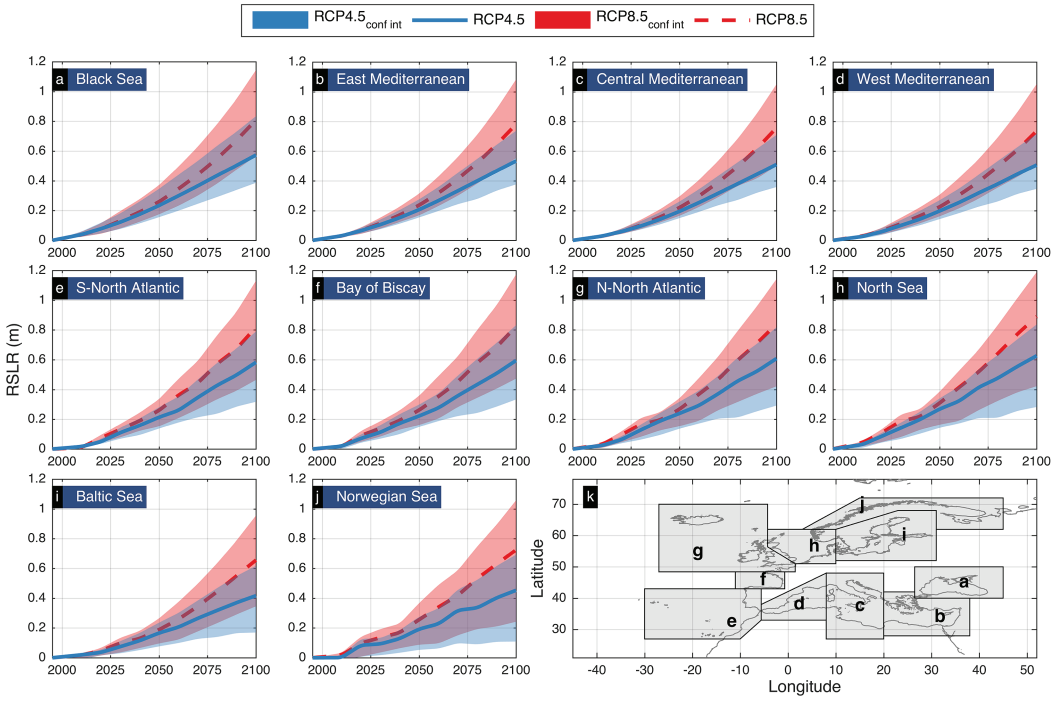

Figure 2. Time evolution of relative sea level rise (RSLR) under Representative Concentration Pathway (RCP)4.5 and RCP8.5. Lines express the ensemble mean and colored patches the inter-model range (defined by the best and worst case scenario). Europe is divided in 10 geographical regions (see k) in order to better reflect the spatial variations of RSLR, where the values shown in (a–j) are averages for each region.

The European coastline was divided in 10 geographical regions in order to identify spatial patterns in the data [*Vousdoukas et al.*, 2016a]. Given the scope of the study which is to give an overview about projected ESL changes in Europe, all values discussed in the manuscript correspond to averages either for each region, or for the entire European coastline.

3. Results

3.1. Relative Sea Level Rise

Projections of RSLR indicate a statistically significant increase in MSL along the entire European coastline (Figure 2). The average RSLR across Europe is projected around 21 and 24 cm by the 2050s under RCP4.5 and RCP8.5, respectively. RSLR is projected to accelerate during the present century under both RCPs, reaching 53 and 77 cm by the year 2100. The largest increases in MSL are projected along North Sea and Atlantic coasts, followed by the Black Sea. The smallest increase is projected for the Baltic Sea, which relates to land uplift known to be active in this area [*Johansson et al.*, 2014]. Overall, model agreement is strong for the RSLR projections (mean CV for Europe of 0.17), with the ensemble spread from the different ice-sheet scenarios nearly doubling that of the GCMs (Figures 3c and 3d). The RSLR projections show higher model agreement for the Mediterranean Sea and the Atlantic coast (Figures 3a and 3b); while uncertainty is higher along the North Sea.

3.2. Tides

The tidal projections show strong agreement, with the ensemble spread of the projected maximum tide tending to increase with RSLR uncertainty toward the end of the century (Figure 4). Projections averaged per European region show natural multi-annual fluctuations in the tidal constituents that appear to dominate any long-term trends related to RSLR. Weak decreasing trends can be discerned for the Bay of Biscay and Northern Europe (Figures 4f–j); however, their amplitude is around 1 cm and can be considered negligible. It is important to highlight that the above findings refer to values averaged over regions and do not consider potential local changes, which can be higher. Further analysis of local tidal dynamics was considered beyond the scope of the present manuscript.

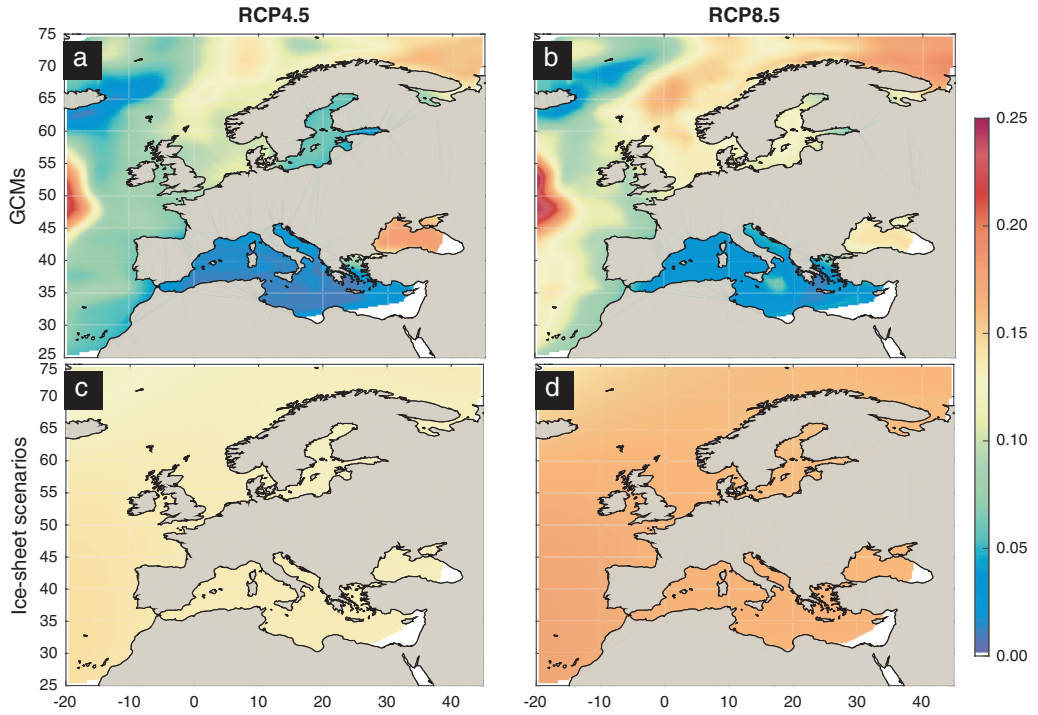

Figure 3. Evaluation of uncertainty in relative sea level rise (RSLR) projections under Representative Concentration Pathway (RCP)4.5 (a, c) and RCP8.5 (b, d). Maps of the RSLR ensemble standard deviation at the year 2100 only from the GCMs (a, b) and only from the ice-sheet scenarios (c, d).

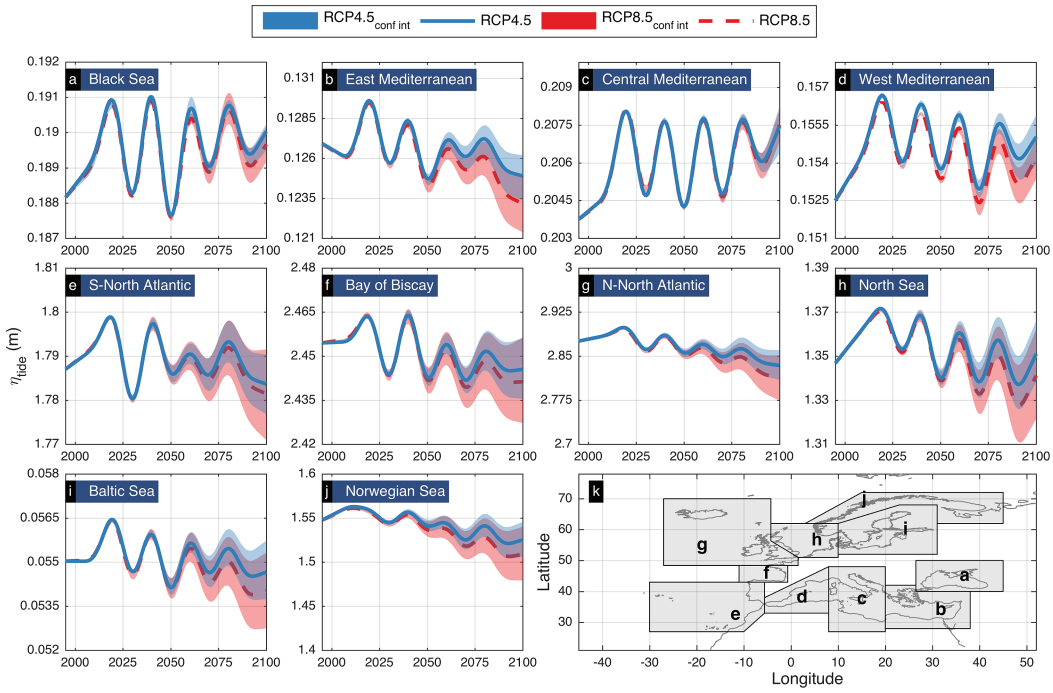

Figure 4. Time evolution of the annual maximum tidal elevation η_{tide} under Representative Concentration Pathway (RCP)4.5 and RCP8.5. Lines express the ensemble mean and colored patches the inter-model range (best-worst relative sea level rise [RSLR] case). In order to understand better the spatial variations of RSLR, the European coastline was divided in 10 geographical regions (see k), and values shown in (a–j) result from averaging all the information from each region.

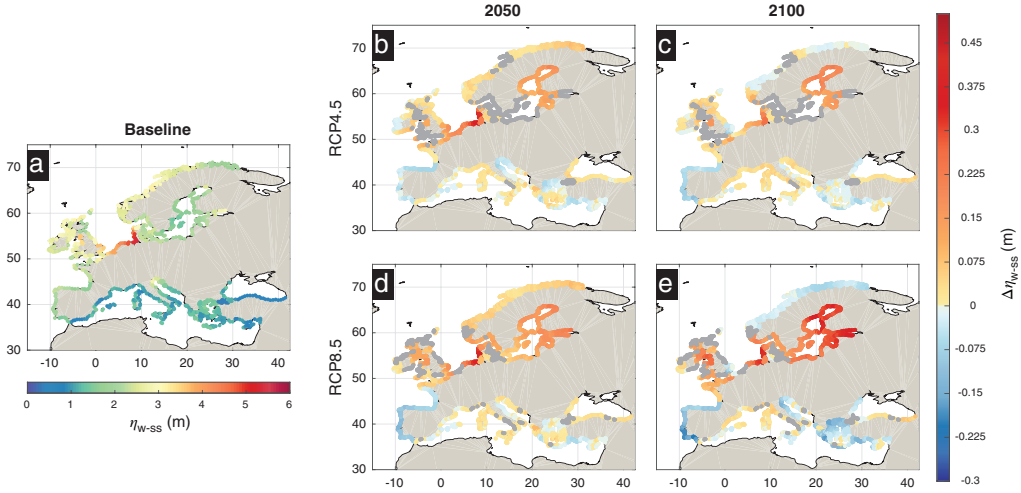

Figure 5. Contribution of climate extremes to extreme sea levels (ESL) along the European coastline and projected changes. Ensemble mean of episodic ESL contributions due to the combined effect of waves and storm surges (η_{w-ss}), expressed as the present-day 100-year η_{w-ss} (a) and projected changes under Representative Concentration Pathway (RCP)4.5 by 2050 (b) and 2100 (c), and under RCP8.5 by 2050 (d) and 2100 (e). Warm/cold colors express an increase/decrease, respectively, while points with high model disagreement are shown in gray (|CV| > 1).

3.3. Climate Extremes

Episodic extremes in waves and storm surges (η_{w-ss}) derived through non-stationary extreme value analysis show no or minor changes along most of the southern European coastline, apart from a significant decrease that is projected for the Portuguese coast and the Gulf of Cadiz (Figure 5). The 100-year η_{w-ss} in this region may lower by 5–8 cm by 2050 and 10–13 cm by 2100 under RCP4.5, and respectively 8–12 and 16–20 cm under RCP8.5. In most regions of northern Europe, an opposite trend emerges, with the highest η_{w-ss} increase projected around the Baltic Sea, and along North Sea coasts of northern Germany and Denmark, projected to reach 35 cm under RCP8.5 towards the end of the century.

The above trends are also present after averaging values per region (Figure 6), and were shown to be statistically significant by Mann–Kendall test. On the other hand, GCM-related inter-model variability and uncertainty is higher compared to the RSLR projections. Climate uncertainty is especially large along several stretches of the UK coast, the western part of the North Sea, and the Kattegat Sea (Figure 5). This is in agreement with previous studies that report uncertainty in projections of waves [*Hemer et al.*, 2013] and storm surges across Europe [*Gaslikova et al.*, 2013] in view of climate change.

3.4. Extreme Sea Levels Along the European Coastline

The ESL_{100}, obtained by combining the projections of RSLR, tides, and the 100-year η_{w-ss}, is shown to increase around 25 cm on average for Europe by 2050 under both scenarios. By the end of the century differences between the two scenarios are more pronounced, with an increase of 57 cm under RCP4.5 and 81 cm under RCP8.5 (Figure 7 and Table 1). The strongest rise in ESL_{100} is projected in the North Sea region with increases up to 75 cm under RCP4.5 and 98 cm under RCP8.5 by the end of the century (Figure 8h). Similar increases are projected for the Atlantic coasts of the UK and Ireland (Figure 8g). Yet still considerable, the lowest increases in ESLs are projected for the Norwegian, the Baltic, and the Mediterranean Sea.

Rising ESLs are mainly driven by RSLR. In general, this tendency is more pronounced under RCP8.5 because of the bigger effect of the concentration pathway on RSLR than on extreme episodic events. Averaged over Europe, the ratio of changes in η_{w-ss} to RSLR ranges between 18% and 9% under RCP4.5, and between 16% and 7% under RCP8.5 (Table 1). For both RCPs, the η_{w-ss} contribution decreases towards the end of the century as RSLR accelerates (Figure 8). Changes in η_{w-ss} are, however, more important for specific regions. This is most prominent for the Baltic Sea, where land uplift results in lower local RSLR, which combined with one of the highest projected η_{w-ss} increases in Europe lead to contribution

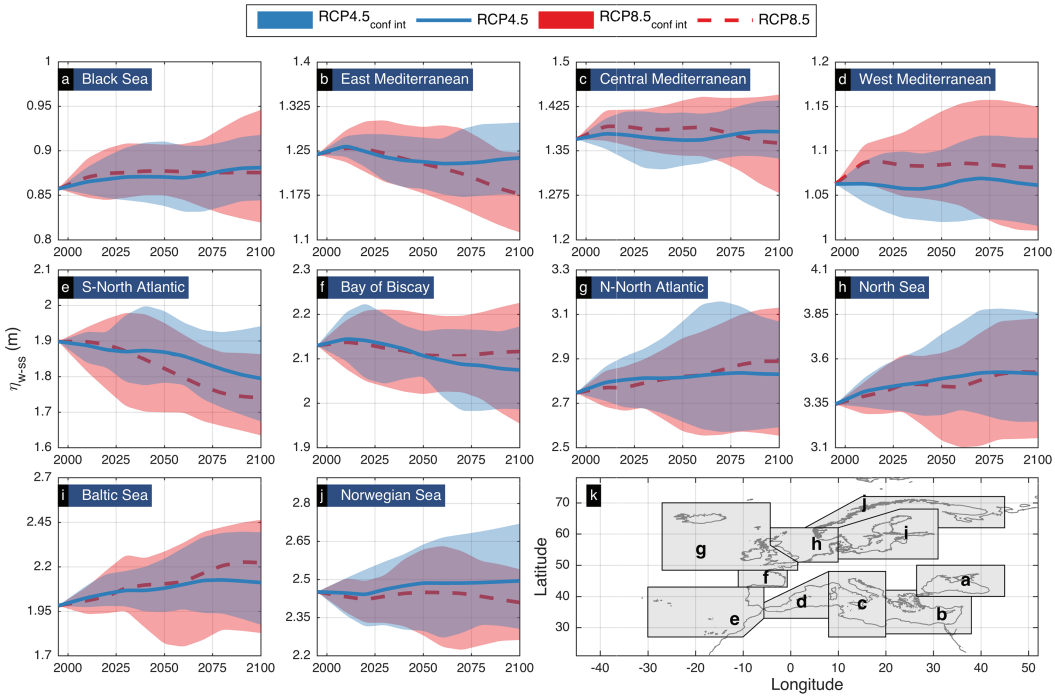

Figure 6. Time evolution of the 100-year η_{w-ss} under Representative Concentration Pathway (RCP)4.5 and RCP8.5. Lines express the ensemble mean and colored patches the inter-model range (best-worst case). In order to understand better the spatial variations of the projections, the European coastline was divided in 10 geographical regions (see k), and values shown in (a–j) result from averaging all the information from each region.

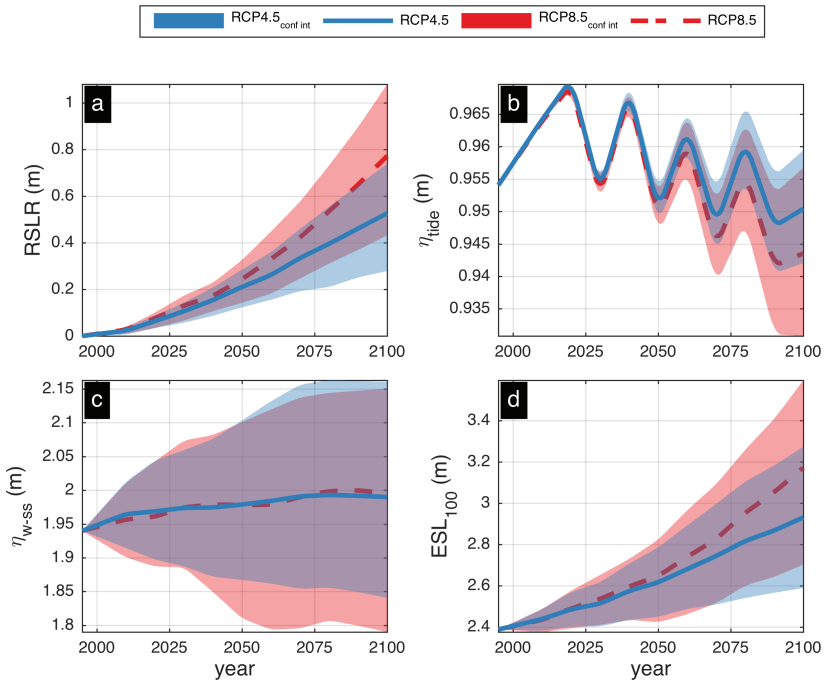

Figure 7. Time evolution of the European mean relative sea level rise (a), maximum tidal elevation (b); 100-year event water level due to waves and storm surges (c) and the combined extreme sea levels (d) under RCP4.5 and RCP8.5. Lines express the ensemble mean and colored patches the inter-model range (best-worst case).

Table 1. Table Summarizing the Projected Absolute and Relative Changes of the 100-Year Event ESL (ΔESL and %ΔESL) Under RCP4.5 and RCP8.5, During the Years 2050 and 2100

	RCP45-2050			RCP45-2100			RCP85-2050			RCP85-2100		
Area	ΔESL (m)	%Δ ESL	%Δ η_{w-ss}	ΔESL (m)	%Δ ESL	%Δη_{w-ss}	ΔESL (m)	%ΔESL	%Δ η_{w-ss}	ΔESL (m)	%Δ ESL	%Δη_{w-ss}
Black Sea	0.25	18.6	7.9	0.60	44.2	4.2	0.27	19.7	5.0	0.81	60.1	1.1
East Mediterranean	0.20	14.3	−5.9	0.53	38.8	−1.1	0.22	16.0	−6.7	0.71	52.3	−8.6
Central Mediterranean	0.19	12.1	−0.8	0.53	33.4	2.5	0.24	14.9	8.6	0.75	47.8	−0.9
West Mediterranean	0.20	15.8	−1.1	0.51	41.0	−0.3	0.24	19.7	9.6	0.75	60.7	2.5
S-North Atlantic	0.18	4.9	−13.8	0.48	12.9	−17.8	0.18	4.9	−29.2	0.66	17.8	−19.4
Bay of Biscay	0.18	4.0	−10.3	0.53	11.6	−9.2	0.22	4.9	−8.2	0.80	17.4	−1.6
N-North Atlantic	0.27	4.7	28.9	0.64	11.3	13.8	0.29	5.2	27.5	0.88	15.7	17.0
North Sea	0.35	7.9	53.5	0.75	17.0	27.4	0.35	7.9	32.4	0.98	22.1	20.2
Baltic Sea	0.27	12.9	58.9	0.55	26.2	31.3	0.31	14.8	65.4	0.88	42.3	36.9
Norwegian Sea	0.21	5.1	18.1	0.46	11.2	9.5	0.23	5.7	−0.8	0.64	15.4	−5.8
Europe	0.25	8.3	18.5	0.57	19.4	9.5	0.27	9.2	15.7	0.81	27.3	7.1

ESLs, extreme sea levels; RCP, Representative Concentration Pathway.
%Δη_{w-ss} expresses how much of the projected change can be attributed to changes in extreme waves and storm surges, considering again the 100-year event.

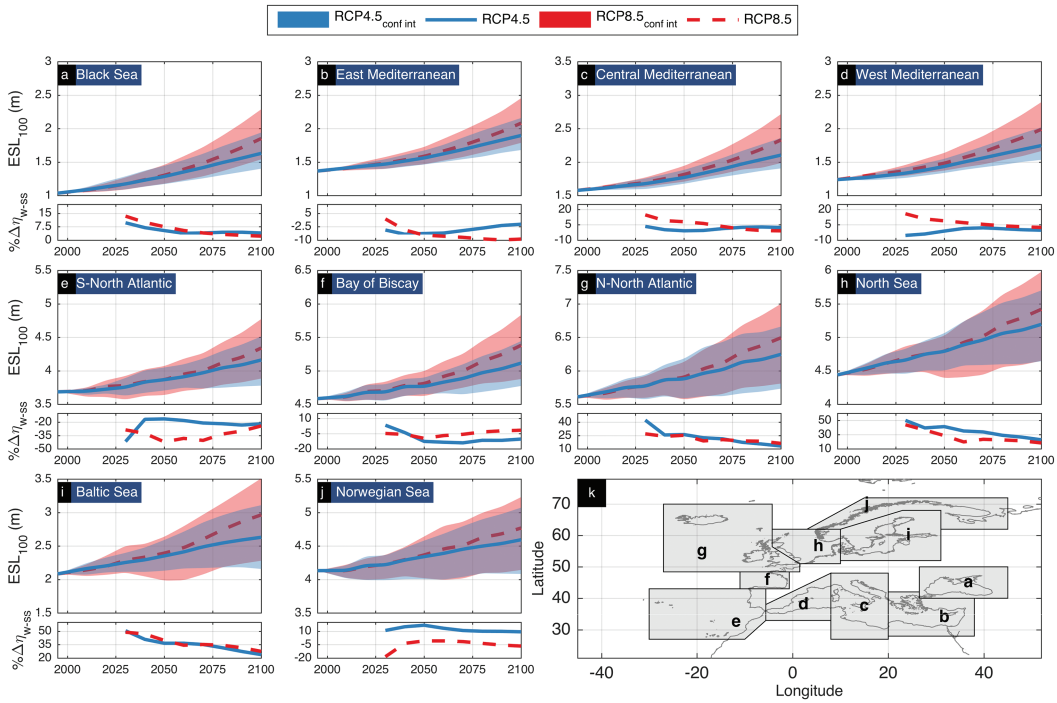

Figure 8. Time evolution of the 100-year event extreme sea levels (ESL) (mean sea level [MSL] + tide + waves + storm surges) under Representative Concentration Pathway (RCP)4.5 and RCP8.5. Lines express the ensemble mean and colored patches the inter-model range (best-worst case). The lower plot shows how much of the projected change in ESL100 is attributed to changes in extreme waves and storm surges %Δη_{w-ss}. Europe is divided in 10 geographical regions (see k) in order to better reflect the spatial variations of relative sea level rise, where the values shown in (a–j) are averages for each region.

values up to 60% of RSLR by mid-century and around 35% by 2100 (Figure 8i). Changes in η_{w-ss} play a significant role in future ESLs also in the North Sea, ranging from 54% of RSLR for RCP4.5 in 2050 to 20% of RSLR under RCP8.5 by 2100 (Figure 8h). Along the Portuguese coast and the Gulf of Cadiz, an opposite effect emerges, with the reduction in η_{w-ss} offsetting RSLR with 30% by mid-century and 20% by 2100 (Figures 8e and 8f, and Table 1). All the above highlight that considering RSLR as the sole driver of increasing risk along the European coastline may lead to bias in the estimation of future potential impacts [*Ruggiero*, 2013].

4. Discussion

4.1. General Remarks

The temporal and spatial scale of the present modeling efforts come with some inevitable compromises in terms of methodology, spatial resolution, and consequently accuracy; especially in comparison with local studies and operational forecasting. Several of these aspects have been thoroughly discussed in Section 4.1 of *Vousdoukas et al.* [2016a], but will be also addressed in the paragraphs to follow.

Previous studies have shown that atmospheric forcing resolution is critical for the predictive skill of ocean models [*Cavaleri and Bertotti*, 2004], especially during short duration/high energy extreme events over large spatial domains [*Conte and Lionello*, 2013; *Calafat et al.*, 2014]. The present projections are based on CMIP5 GCMs, which come with a lower spatial resolution compared with Regional Climate Models (RCMs) available from EURO-CORDEX. The reasons that GCMs were considered as the most appropriate solution are (i) RCM data were available only with a 24-h time step, in comparison with 6-h GCM projections, and preliminary model runs showed that 24 h was not sufficient to resolve marine storms; (ii) RCMs do not resolve atmospheric conditions along the largest extent of the Atlantic Ocean; which are very important for storm surges and in particular for waves along Europe's Atlantic coast. A potential solution, applied for regional/local scale studies, would be to downscale atmospheric forcing using a finer model. However, the latter was not feasible in the present case due to the size of the domain and the related computational costs. Moreover, previous studies have demonstrated that large-scale simulations are capable of predicting changes in extreme storm surge levels without previous downscaling [*Howard et al.*, 2010].

The GCMs considered for SLR projections and climate extremes simulations are not consistent, an inevitable compromise since not all GCMs were available at the CMIP5 database during the period the modeling was taking place. Even though this may initially appear as a methodological inconsistency, we believe that it is of minor importance since GCMs provide only projections of SLR from thermal expansion, omitting all the other components, e.g., ice-sheets and glaciers. As described in Section 2.2, the missing components are estimated separately and added linearly at a later stage, considering three different scenarios [*Hinkel et al.*, 2014; *Mengel et al.*, 2016]. The latter implies that it is not possible to have one ESL projection per GCM, but rather a set of three, and that was the reason that the RSLR ensemble mean and inter-model range were estimated separately. Moreover, most studies project that thermal expansion becomes of secondary importance toward the end of the century [*Marzeion et al.*, 2012; *Jackson and Jevrejeva*, 2016], rendering the selection of GCMs for SLR projections less significant with time.

Our modeling approach does not resolve nonlinear interactions between waves, storm surge, and tides. Instead each ESL component is simulated separately and then they are all summed linearly to produce ESLs. Water level variations are important both for waves [*Vousdoukas et al.*, 2012] and storm surges [*Arns et al.*, 2015], as the depth modulates the bottom friction and the water extent. Moreover, tidal currents interact with the wind-driven circulation [*Zijl et al.*, 2013] and both are interacting with waves [*Roland et al.*, 2012]. All these processes introduce nonlinear effects, which may explain, along with the model resolution, part of the errors observed in the validation results. However, these shortcomings are inevitable given the current modeling capabilities, both in terms of computational power and software. According to the authors' knowledge, there is no continental-scale modeling system that simulates waves and ocean circulation in coupled mode. Few systems run on regional scales [*Warner et al.*, 2010; *Bertin et al.*, 2012; *Zhang*

et al., 2013; *Hashemi et al.*, 2015; *Sembiring et al.*, 2015], producing short-term forecasts with simulation horizons that are orders of magnitude lower than in the case of climate change projections. For the above reasons, the approach of linearly adding ESL components has been used in similar studies and has been showing to result in acceptable accuracy [*Lowe and Gregory*, 2005; *Sterl et al.*, 2009; *Howard et al.*, 2010; *Losada et al.*, 2013].

Another reason that coupled simulations were avoided is related to the fact that tidal variations modulate ESLs, with extremes occurring only during high tides. Whereas the timing of the tides is to a large extent deterministic, this is not the case for the timing of the climate extremes obtained from CMIP5 GCMs. For the same emission forcing, there is substantial variability in the sequences of meteorological conditions among GCMs, as is the case among different realizations from the same GCM. As a result, reproducing the ESL probability density function for a given scenario would require to consider a set of simulations were the timing of the tides would vary in a Monte Carlo fashion. Such an approach would add to the already intense computational loads, practically rendering the study not feasible.

Waves are a very important coastal hazard component. A detailed discussion on the assumptions/limitations of the present approach related to wave contributions to coastal hazard, can be found in *Vousdoukas et al.* [2016b]. Among the assumptions is considering wave setup as 20% of the significant wave height, an approach that neglects several wave properties, such as directional spectra and the effect of nearshore bathymetry. More elaborate ways to estimate wave setup exist, which apart from the significant wave height also consider the wave period, length, and nearshore slope of the sea bottom. The bathymetry along the last tens of meters near the coast is critical for wave shoaling/breaking processes that drive local water levels, i.e., wave setup and runup, as well as for morphological changes and erosion. However, information about the nearshore bathymetry and/or the slope is not available at European scale at the resolution required to resolve such detailed processes. The applied approach for wave setup was chosen as the best compromise between computational effort and local accuracy given that the scope of the present study is to assess general ESL trends along Europe's coasts rather than to simulate local processes with high accuracy. In that respect, validation efforts overall resulted in acceptable errors.

The strength of the projected changes is more enhanced by using a six-member climate model ensemble and considering the ensemble mean only when model agreement is acceptable through a threshold in the coefficient of variation. At the same time, the subtraction between baseline and projected values cancels out many possible shortcomings in the climate extremes simulations. The discussion of the modeling-strategy induced uncertainty aims to inform the reader and potential user of the dataset that the relative accuracy of the ESL components values should be considered in the range of 10–20%, although locally errors could be higher.

The present study is based on an extensive dataset covering projections of all ESL components during the present century, and such information could potentially provide several scientific insights, which are not presently addressed. The present contribution has been focussed mostly on statistical and methodological aspects leading to reliable projections of ESLs; while further data interpretation takes place in separate studies [e.g., *Vousdoukas et al.*, 2016a, 2016b; *L. Mentaschi et al.*, 2017]. Moreover, the fact that the dataset is openly available allows the scientific community to address unexplored aspects of the dynamics of ESL components during this century.

4.2. Projected Changes in ESL Components

Projections of wave action along the European coastline do not allow drawing general conclusions. Previous studies project a decrease [*Charles et al.*, 2012; *Perez et al.*, 2015], or no significant changes in significant wave heights, but changes in direction [*de Winter et al.*, 2012; *Casas-Prat and Sierra*, 2013; *Hemer et al.*, 2013; *Semedo et al.*, 2013]. Still some studies report increases that are either local [*Mori et al.*, 2013; *Dobrynin et al.*, 2015], or related only to the winter season [*Zacharioudaki et al.*, 2011; *Fan et al.*, 2014], or only to the extremes [*Brown et al.*, 2012]. A comparison with the present dataset is not straightforward as most previous studies focus on SRES scenarios and discuss changes in certain percentiles; in contrast to the present study, which focusses on RCPs and on extremes. Similarly to the present findings, previous projections of storm surges

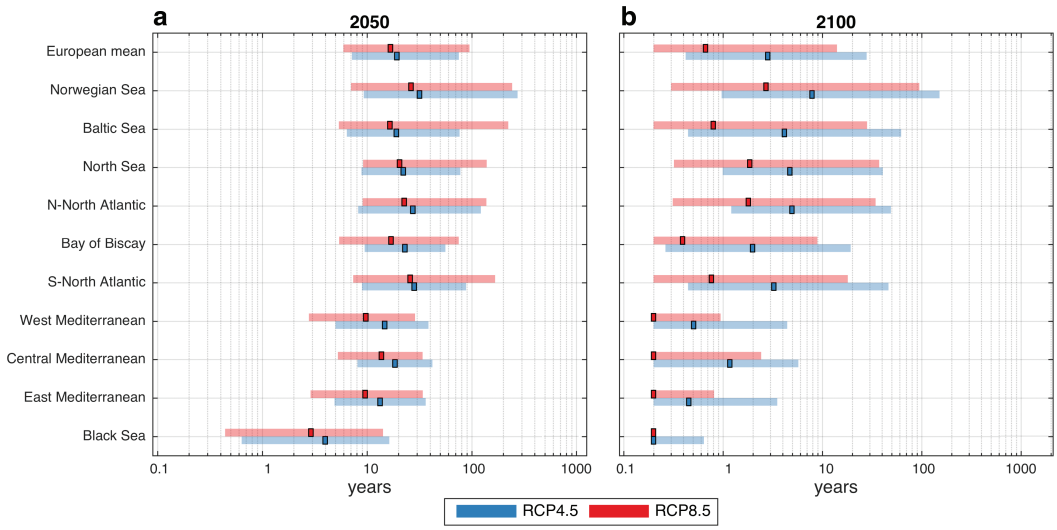

Figure 9. Return period of the present day 100-year extreme sea levels under Representative Concentration Pathway (RCP)4.5 and RCP8.5 in 2050 (a) and 2100 (b). Colored boxes express the ensemble mean value and colored patches the inter-model variability (best-worst case). The values shown are averages along the European coastline as well as along the coasts of 10 geographical regions (as in Figures 1 and 3).

predict an increase in storm surge levels along coastal stretches of north Europe [*Meier*, 2006; *Woth et al.*, 2006; *Debernard and Røed*, 2008; *Lowe et al.*, 2009; *Weisse et al.*, 2009; *Brown et al.*, 2010; *Brown et al.*, 2012; *Gräwe and Burchard*, 2012; *Gaslikova et al.*, 2013; *Howard et al.*, 2014]; and decreasing, or no strong trends for south Europe [*Marcos et al.*, 2011; *Jordà et al.*, 2012; *Marcos et al.*, 2012; *Conte and Lionello*, 2013; *Androulidakis et al.*, 2015].

Less consistent are the projections of the effect of SLR on tides, with previous studies not reaching consensus. Even though there is reported evidence of changes in tidal constituents in the 20th century [*Mawdsley et al.*, 2015], the attribution of reported changes remains yet unresolved [*Woodworth*, 2010]. The present results corroborate findings of previous studies suggesting negligible effects on tides [*Lowe et al.*, 2001; *Sterl et al.*, 2009] for RSLR scenarios like the ones presently studied (RSLR < 1.2 m), although that more recent efforts have shown that RSLR can affect tides locally even for RSLR < 1.0 m [*Pelling and Mattias Green*, 2014; *Arns et al.*, 2015]. Pickering *et al.* [2012] further suggest that tides could be affected by extreme SLR scenarios (RSLR > 2.0 m).

4.3. Socio-Economic Implications

The projected rise in ESLs constitutes a serious threat to European coastal societies. Their safety and resilience depends on the effectiveness of natural and man-made coastal flood protection, i.e., the capacity of the coastal zone to act as a buffer and absorb ocean energy through complex wave shoaling and breaking processes [*Vousdoukas et al.*, 2012]. Taking into account flood protection standards in place and uncertainty in their probability of failure, around 5 million people could potentially be affected by the present day ESL_{100} [*Vousdoukas et al.*, 2016b]. Present findings imply that averaged over Europe's coastlines, the latter is projected to occur approximately every 11 years by 2050, and every 3 and 1 years by 2100 under RCP4.5 and RCP8.5, respectively (Figure 9 and Table 2). Hence, the 5 million Europeans currently at risk to be flooded by sea water once every 100 years, may be flooded on an almost annual basis by the end of this century. Some regions are projected to experience an even higher increase in the frequency of occurrence of extreme events, most notably along the Mediterranean and the Black Sea, where the present day 100-year ESL is projected to occur several times a year. Such increase in frequency of events that today are considered as exceptional will likely push existing coastal protection structures beyond their design limits [*Sierra and Casas-Prat*, 2014], rendering a large part of Europe's coastal zones exposed to intermittent flood hazard. These findings stress the need to timely develop and implement appropriate adaptation measures.

Table 2. Return Period of the Present Day 100- and 1000-Year ESL (MSL + Tide + Waves + Storm Surges) Under RCP4.5 and RCP8.5 in the Years 2050 and 2100, Under RCP4.5 and RCP8.5

	$T_r = 100$				$T_r = 1000$			
	RCP4.5		RCP8.5		RCP4.5		RCP8.5	
	2050	2100	2050	2100	2050	2100	2050	2100
Black Sea	3.7	0.1	2.6	0.1	35.4	0.3	25.9	0.1
East Mediterranean	13.4	0.5	9.6	0.2	88.0	2.9	67.8	0.3
Central Mediterranean	18.5	1.2	13.8	0.2	159.0	8.4	99.0	1.2
West Mediterranean	14.8	0.5	9.8	0.2	157.4	6.9	94.5	0.6
S-North Atlantic	28.3	3.3	25.9	0.8	185.5	18.5	193.6	4.6
Bay of Biscay	23.0	2.0	17.0	0.4	138.5	8.4	91.5	1.6
N-North Atlantic	27.4	4.9	22.7	1.8	167.4	23.9	147.5	8.0
North Sea	22.2	4.7	20.5	1.9	141.2	22.9	142.7	8.9
Baltic Sea	19.1	4.2	16.6	0.8	132.5	22.7	96.5	4.1
Norwegian Sea	31.8	7.9	26.3	2.7	200.3	43.6	178.9	15.2
European-mean	19.3	2.8	16.8	0.7	136.2	15.2	107.2	3.6

ESLs, extreme sea levels; MSL, mean sea level; RCP, Representative Concentration Pathway.
Values express the ensemble mean value and in order to understand better the spatial variations of ESL, the values shown are averaged along the European coastline, as well as along 10 geographical regions.

5. Conclusions

The present contribution provides the first pan-European assessment of the evolution of ESLs in view of climate change considering all driving components. Datasets of the ESL components (SLR, tides, waves, storm surges) were generated by dynamic simulations forced by a multi-GCM ensemble. For each component, a reanalysis was carried out for the baseline period and projections were made until the end of the century considering RCP4.5 and RCP8.5.

Projections of RSLR indicate a statistically significant increase in MSL along the entire European coastline, around 21 and 24 cm by the 2050s under RCP4.5 and RCP8.5, respectively, to reach 53 and 77 cm by the end of the century. Tidal simulations show no significant control of RSLR on tidal elevation throughout the century at regional scale; however, this does not exclude potential local effects.

Episodic extremes in waves and storm surges (η_{w-ss}) show no or minor changes along most of the southern European coastline, apart from an important decrease that is projected for the Portuguese coast and the Gulf of Cadiz, where the 100-year η_{w-ss} may lower by 5–12 cm by 2050 and 10–20 cm by 2100. In most regions of northern Europe, an opposite trend emerges, with the highest η_{w-ss} increase projected around the Baltic Sea, and along North Sea coasts of northern Germany and Denmark, projected to reach 35 cm under RCP8.5 towards the end of the century.

The ESL_{100}, obtained by combining the projections of RSLR, tides, and the 100-year η_{w-ss}, is shown to increase around 25 cm on average for Europe by 2050 under both scenarios. By the end of the century, differences between the two scenarios are more pronounced, with an increase of 57 cm under RCP4.5 and 81 cm under RCP8.5. The strongest rise in ESL_{100} is projected in the North Sea region with increases up to 75 cm under RCP4.5 and 98 cm under RCP8.5 by the end of the century. Similar increase is projected for the Atlantic coasts of the UK and Ireland, and considerable increases are projected for the Norwegian, the Baltic, and the Mediterranean Sea.

Rising ESLs are mainly driven by RSLR, especially under RCP8.5. Averaged over Europe, the ratio of changes in η_{w-ss} to RSLR ranges between 18% and 9% under RCP4.5, and between 16% and 7% under RCP8.5. For both RCPs, the contribution decreases toward the end of the century as RSLR accelerates. Important contribution from η_{w-ss} is projected along the Baltic Sea, reaching values up to 65% of RSLR by mid-century and around 35% by 2100. Substantial η_{w-ss} contributions in rising future ESLs are also discerned for the North Sea, ranging from 54% of RSLR for RCP4.5 in 2050 to 20% of RSLR under RCP8.5 by 2100. Along the Portuguese coast and the Gulf of Cadiz, an opposite effect emerges, with the reduction in η_{w-ss} offsetting RSLR with 30% by mid-century and 20% by 2100.

The present findings indicate that by the end of this century, 5 million Europeans currently under threat of a 100-year ESL could be annually at risk from coastal flooding under RCP8.5, and every 2–3 years under RCP4.5. The presented dataset is available through the JRC open access database from this link: http://data.jrc.ec.europa.eu/collection/LISCOAST.

Acknowledgments
The research leading to these results has received funding from the EU Seventh Framework Programme FP7/2007-2013 under grant agreement no. 603864 (HELIX: "High-End cLimate Impacts and eXtremes"; http://www.helixclimate.eu), from DG CLIMA of the European Commission as part of the PESETA3 project, as well as from the JRC of the European Commission as part of the CoastAlRisk project.

Appendix A

A1. Model Validation

The performance evaluation was carried out on a time interval of 35 years between 1980 and 2014, and WWIII was forced by ERA-Interim reanalysis wind data with a spatial resolution of about 80 km and a time step of 12 h. Due to a tendency to underestimate the surface winds by ERA-Interim with respect to other reanalysis such as CFSR, the model was calibrated to eliminate a systematic bias of significant wave height following *Rascle and Ardhuin* [2013].

The validation was performed comparing the modeled H_s with the one measured by altimeter data provided by 6 different satellites: ERS-2, ENVISAT, Jason 1 and 2, Cryosat 2, and SARAL-AltiKa. Satellite data are provided by the Globwave dataset [*Queffeulou and Croizé-Fillon*, 2014]. A further validation was carried out using the measurements provided by buoys located mainly in Europe and America. The set of buoy datasets include the American National Data Buoy Center (NDBC), the dataset Seadatanet, the Italian Rete Ondametrica Nazionale (RON), the Spanish buoys of the REDEXT network and the Greek network Poseidon. The employment of buoy measurements allowed an assessment of the modeled mean period and direction.

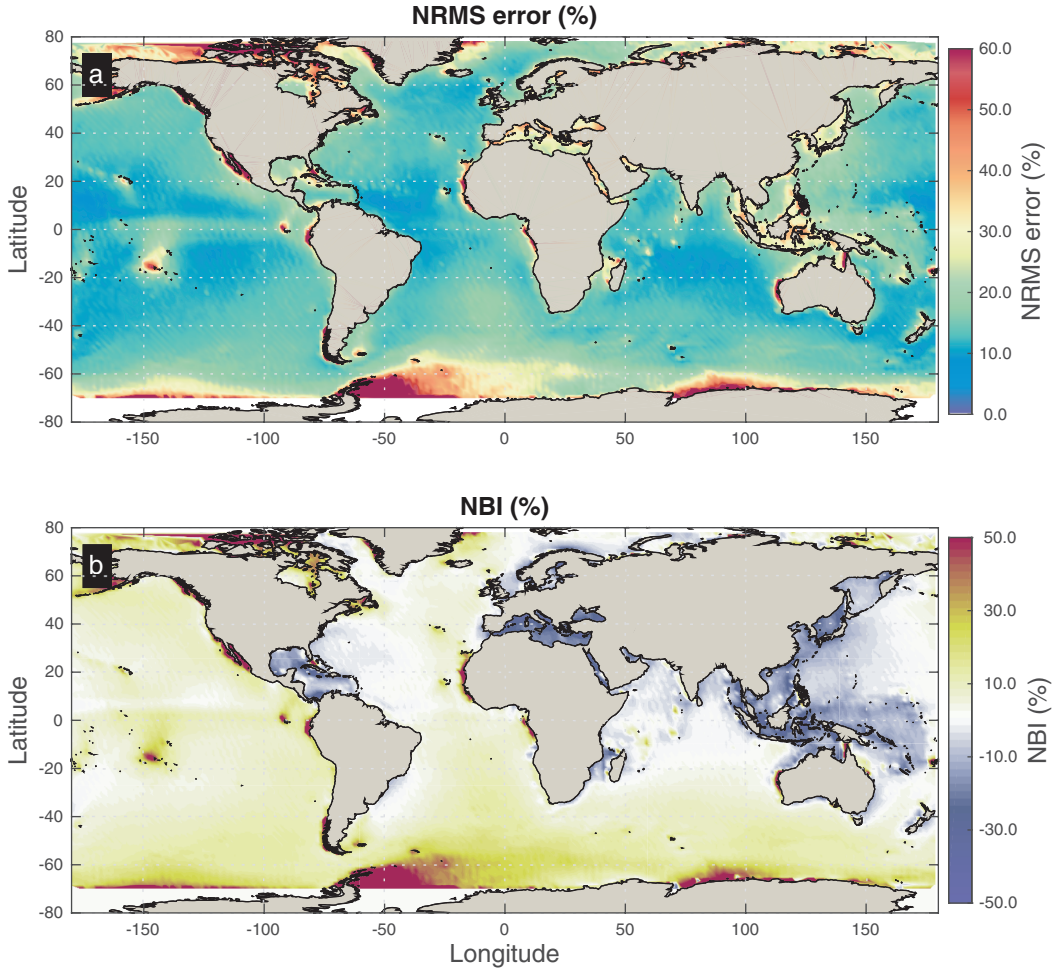

Figure A1. Wave model validation against satellite data: maps showing Normalized Root Mean Square (NRMS) error (a) and Normalized BIAS (NBI) (b) of significant wave height.

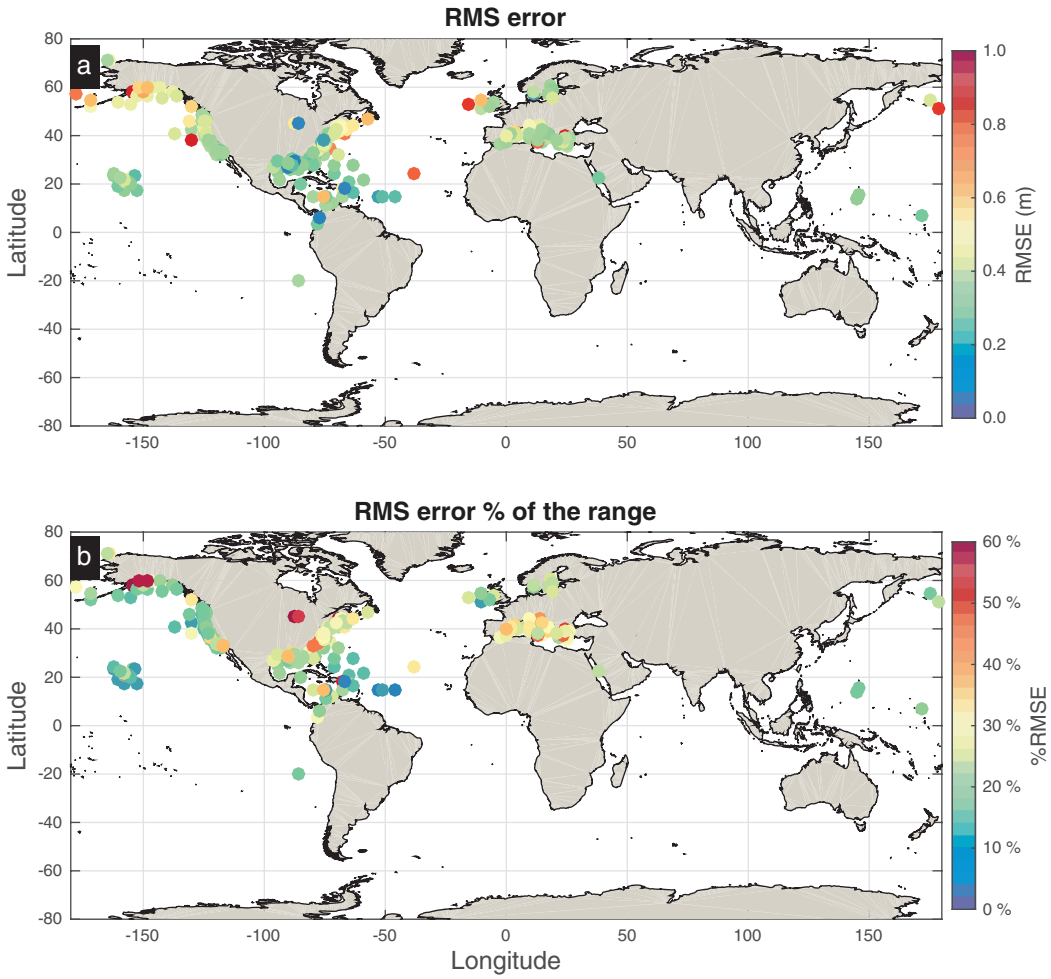

Figure A2. Wave model validation performance: scatter plot showing Root Mean Square (RMS) error in m (a) and as a percentage of the H_s range (b) for all the available wave measuring stations for significant wave height.

The comparison between simulated and observed values was carried out for significant wave height and mean period using the following error indicators:

- Normalized bias (NBI)

$$\mathrm{NBI} = \frac{\sum S_i - O_i}{\sum O_i} \tag{A1}$$

where S_i and O_i are simulations and observations, respectively. This is an indicator of the average component of the error and a value closer to zero indicates a better simulation.

- Normalized root mean square error (NRMSE)

$$\mathrm{NRMSE} = \sqrt{\frac{\sum (S_i - O_i)^2}{\sum O_i^2}} \tag{A2}$$

NRMSE combines information about the average and the scatter components of the error, and a value closer to zero indicates a better simulation.

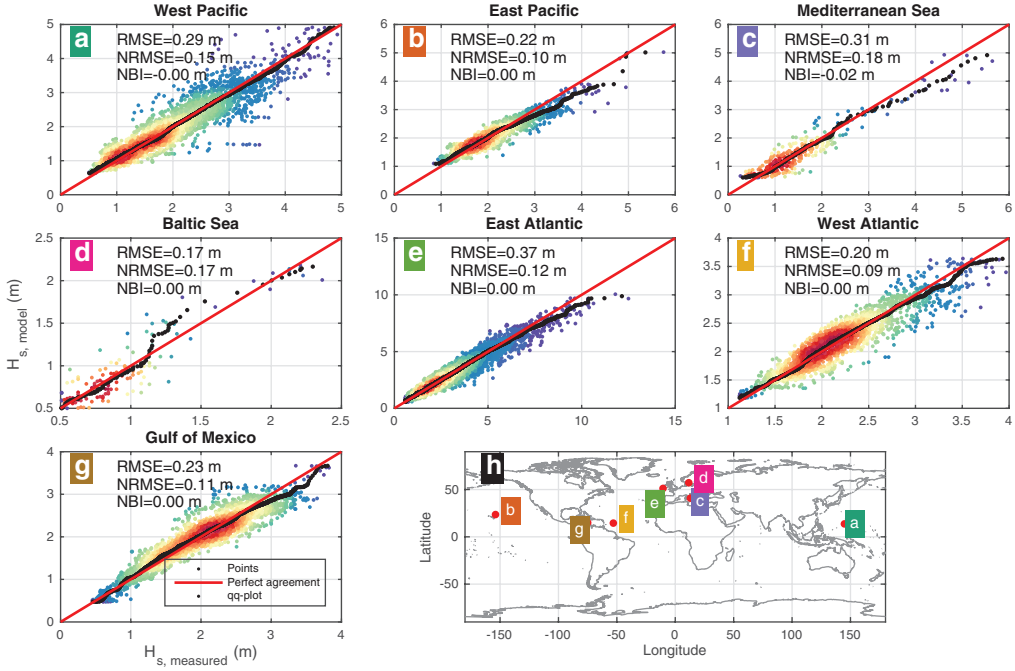

Figure A3. Wave model validation against buoy data. (a–g) Scatter plots comparing simulated against measured significant wave heights at different locations worldwide; with red lines expressing the perfect agreement function, and black dots showing the q–q plots. A world map with all the validation points is also shown (h).

For the mean direction these indicators have been redefined as

$$\mathrm{NBI}_\theta = \sum \frac{\mathrm{mod}_{-\pi,\pi}\left(\theta_{S_i} - \theta_{O_i}\right)}{2\pi N} \tag{A3}$$

$$\mathrm{NMRSE}_\theta = \sqrt{\sum \frac{\left[\mathrm{mod}_{-\pi,\pi}\left(\theta_{S_i} - \theta_{O_i}\right)\right]^2}{2\pi N}} \tag{A4}$$

where the modulo operator $\mathrm{mod}_{-\pi,\pi}$ indicates that if $\left(\theta_{S_i} - \theta_{O_i}\right) > \pi$ a 2π angle is subtracted to the difference, if $\left(\theta_{S_i} - \theta_{O_i}\right) < -\pi$ a 2π angle is added to the difference.

Since the spatial/temporal resolution of satellite data along the satellite tracks is much higher than that of the model, satellite data have been binned over latitudinal spans of 1.5° and averaged, before comparing them with model data.

A2. Results

In general, the agreement between modeled significant wave height and satellite observations is satisfactory, with an overall NBI of about 2% and a NRMSE of about 14%. The employment of satellite data for significant wave height allowed a spatial evaluation of model performance, which is illustrated in Figure A1. Model results are generally optimal in open oceans with values of NBI close to zero and NRMSE below 10% in many areas. In enclosed or semi-enclosed seas, notably the Mediterranean Sea, the Sea of Japan, some parts of the sea around Indonesia and of the Baltic Sea, results are characterized by strong negative bias. This is mainly due to the fact that while in open oceans wave dynamics are dominated by swell, in enclosed and semi-enclosed basins local conditions and mesoscale dynamics, i.e., dynamics on length scales in the order of 100 km or less, attain an important role [*Mentaschi et al.*, 2015]. This aspect is particularly relevant in areas characterized by a complex orography such as the Mediterranean Sea, where low-resolution atmospheric forcing is often associated with a smoothing of sharp gradients of physical patterns. The inability of low-resolution models to represent properly mesoscale dynamics can be a major issue in operational/forecasting systems that can be partially overcome increasing the space-time resolution.

Table A1. Groups of Buoys and Overall Error Indicators for Significant Wave Height H_s, Mean Period T_{02} and Mean Direction θ_m

Buoy Group	*N* Buoys (H_s, T_{02})	NBI_{Hs} (%)	$NRMSE_{Hs}$ (%)	NBI_{Tm} (%)	$NRMSE_{Tm}$ (%)	*N* Buoys (θ_m)	NBI_θ	$NRMSE_\theta$
W Pacific	3	0.4	21.6	0.7	12.3	0	N.D.	N.D.
E Pacific	83	7.2	19.2	5.0	17.8	75	1.1%	9.5%
Mediterranean	34	−29.5	43.5	−17.7%	27.3%	34	−3.8%	15.6%
Baltic	6	−22.7	30.3	−7.9	18.2	6	−1.5%	12.2%
E Atlantic	7	−4.2	15.8	−1.9	24.1	0	N.D.	N.D.
W Atlantic	94	2.7	27.4	0.5	18.0	45	−2.9%	10.1%
Mexico Gulf	41	−15.4	28.3	−6.2	16.4	20	−0.6%	8.0%

However, this study focuses on long-term trends related to the global scale/synoptic dynamics that GCMs are able to capture, and the resolution applied is considered sufficient.

The comparison of model results with buoy measurements for significant wave height results in values of NBI and NRMSE similar to those found with satellites (Figure A2). The performance evaluation versus buoy measurements was carried out considering nine different groups of buoys selected on the basis of the geographical position of each buoy (Figure A3). In deep water in the oceans, the skills are generally good; while model skill in enclosed basins is often affected by negative bias of significant wave height, for the same reasons discussed for satellite data. The inability of the model to simulate small-scale coastal dynamics affects the skills of the simulations versus buoys close to coastline.

In the validation procedure, the mean period measured by the buoy was compared with the mean period T_{02} computed by the model, which is an estimation of the zero-crossing period of waves [*Tucker and Pitt*, 2001]. The comparison between simulated and measured mean period T_{02} and mean direction θ_m is generally good, with a tendency to underestimate T_{02} in enclosed basins such as the Mediterranean Sea, the Baltic Sea and the Gulf of Mexico. Normalized Root Mean Square Error (NRMSE) values for the wave period are within the 12–28% range and the absolute Normalized BIAS (NBIAS) is below 1% for most areas, but reach 18% for some enclosed seas (Table A1). The absolute NBIAS for the direction is below 4% for all areas, while NRMSE values vary form 8% to 16%.

References

Alfieri, L., P. Burek, L. Feyen, and G. Forzieri (2015), Global warming increases the frequency of river floods in Europe, *Hydrol. Earth Syst. Sci.*, *19*, 2247–2260, doi:10.5194/hess-19-2247-2015.

Androulidakis, Y. S., K. D. Kombiadou, C. V. Makris, V. N. Baltikas, and Y. N. Krestenitis (2015), Storm surges in the Mediterranean Sea: Variability and trends under future climatic conditions, *Dyn. Atmos. Oceans*, *71*, 56–82, doi:10.1016/j.dynatmoce.2015.06.001.

Ardhuin, F., et al. (2010), Semiempirical dissipation source functions for ocean waves. Part I: Definition, calibration, and validation, *J. Phys. Oceanogr.*, *40*(9), 1917–1941, doi:10.1175/2010jpo4324.1.

Arns, A., T. Wahl, S. Dangendorf, and J. Jensen (2015), The impact of sea level rise on storm surge water levels in the northern part of the German Bight, *Coast. Eng.*, *96*, 118–131, doi:10.1016/j.coastaleng.2014.12.002.

Bertin, X., N. Bruneau, J.-F. Breilh, A. B. Fortunato, and M. Karpytchev (2012), Importance of wave age and resonance in storm surges: The case Xynthia, Bay of Biscay, *Ocean Model.*, *42*, 16–30, doi:10.1016/j.ocemod.2011.11.001.

Bidlot, J., P. Janssen, and S. Abdalla (2007), A revised formulation of ocean wave dissipation and its model impact, *Rep.*, ECMWF, Reading, U. K.

Bowen, A. J., D. L. Inman, and V. P. Simmons (1968), Wave 'set-down' and set-up, *J. Geophys. Res.*, *73*, 2569–2577, doi:10.1029/JB073i008p02569.

Brown, J., A. Souza, and J. Wolf (2010), Surge modelling in the eastern Irish Sea: Present and future storm impact, *Ocean Dyn.*, *60*(2), 227–236, doi:10.1007/s10236-009-0248-8.

Brown, J., J. Wolf, and A. Souza (2012), Past to future extreme events in Liverpool Bay: Model projections from 1960–2100, *Clim. Change*, *111*(2), 365–391, doi:10.1007/s10584-011-0145-2.

Brown, S., R. J. Nicholls, J. A. Lowe, and J. Hinkel (2013), Spatial variations of sea-level rise and impacts: An application of DIVA, *Clim. Change*, *134*(3), 403–416, doi:10.1007/s10584-013-0925-y.

Calafat, F. M., E. Avgoustoglou, G. Jordà, H. Flocas, G. Zodiatis, M. N. Tsimplis, and J. Kouroutzoglou (2014), The ability of a barotropic model to simulate sea level extremes of meteorological origin in the Mediterranean Sea, including those caused by explosive cyclones, *J. Geophys. Res. Oceans*, *119*(11), 7840–7853, doi:10.1002/2014JC010360.

Carson, M., A. Köhl, D. Stammer, A. B. A. Slangen, C. A. Katsman, R. S. W. van de Wal, J. Church, and N. White (2016), Coastal sea level changes, observed and projected during the 20th and 21st century, *Clim. Change*, *134*(1), 269–281, doi:10.1007/s10584-015-1520-1.

Casas-Prat, M., and J. P. Sierra (2013), Projected future wave climate in the NW Mediterranean Sea, *J. Geophys. Res. Oceans*, *118*(7), 3548–3568, doi:10.1002/JGRC.20233.

Cavaleri, L., and L. Bertotti (2004), Accuracy of the modelled wind and wave fields in enclosed seas, *Tellus A*, *56*(2), 167–175, doi:10.3402/tellusa.v56i2.14398.
Charles, E., D. Idier, P. Delecluse, M. Déqué, and G. Le Cozannet (2012), Climate change impact on waves in the Bay of Biscay, France, *Ocean Dyn.*, *62*(6), 831–848, doi:10.1007/s10236-012-0534-8.
Chen, X., Y. Feng, and N. E. Huang (2014), Global sea level trend during 1993–2012, *Global Planet. Change*, *112*, 26–32, doi:10.1016/j.gloplacha.2013.11.001.
Ciavola, P., O. Ferreira, P. Haerens, M. Van Koningsveld, and C. Armaroli (2011), Storm impacts along European coastlines. Part 2: Lessons learned from the MICORE project, *Environ. Sci. Policy*, *14*(7), 924–933, doi:10.1016/j.envsci.2011.05.009.
Conte, D., and P. Lionello (2013), Characteristics of large positive and negative surges in the Mediterranean Sea and their attenuation in future climate scenarios, *Global Planet. Change*, *111*, 159–173, doi:10.1016/j.gloplacha.2013.09.006.
Cutter, S. L., and M. Gall (2015), Sendai targets at risk, *Nat. Clim. Change*, *5*(8), 707–709, doi:10.1038/nclimate2718.
Dangendorf, S., D. Rybski, C. Mudersbach, A. Müller, E. Kaufmann, E. Zorita, and J. Jensen (2014), Evidence for long-term memory in sea level, *Geophys. Res. Lett.*, *41*(15), 5530–5537, doi:10.1002/2014GL060538.
Debernard, J. B., and L. P. Røed (2008), Future wind, wave and storm surge climate in the Northern Seas: A revisit, *Tellus A*, *60*(3), 427–438, doi:10.1111/j.1600-0870.2008.00312.x.
Dobrynin, M., J. Murawski, J. Baehr, and T. Ilyina (2015), Detection and attribution of climate change signal in ocean wind waves, *J. Clim.*, *28*(4), 1578–1591, doi:10.1175/jcli-d-13-00664.1.
Egbert, G. D., and S. Y. Erofeeva (2002), Efficient inverse modeling of barotropic ocean tides, *J. Atmos. Oceanic Tech.*, *19*(2), 183–204, doi:10.1175/1520-0426(2002)019<0183:eimobo>2.0.co;2.
European Commission (2007), The EU Floods Directive, [Available at http://ec.europa.eu/environment/water/flood_risk/.]
European Commission (2013), EU Climate Change Adaptation Strategy, [Available at http://ec.europa.eu/clima/policies/adaptation/what/documentation_en.htm.]
Fan, Y., S.-J. Lin, S. M. Griffies, and M. A. Hemer (2014), Simulated global swell and wind-sea climate and their responses to anthropogenic climate change at the end of the twenty-first century, *J. Clim.*, *27*(10), 3516–3536, doi:10.1175/jcli-d-13-00198.1.
Gaslikova, L., I. Grabemann, and N. Groll (2013), Changes in North Sea storm surge conditions for four transient future climate realizations, *Nat. Hazards*, *66*(3), 1501–1518, doi:10.1007/s11069-012-0279-1.
Gräwe, U., and H. Burchard (2012), Storm surges in the Western Baltic Sea: The present and a possible future, *Clim. Dyn.*, *39*(1–2), 165–183, doi:10.1007/s00382-011-1185-z.
Hashemi, M. R., S. P. Neill, and A. G. Davies (2015), A coupled tide-wave model for the NW European shelf seas, *Geophys. Astrophys. Fluid Dyn.*, *109*(3), 234–253, doi:10.1080/03091929.2014.944909.
Hauer, M. E., J. M. Evans, and D. R. Mishra (2016), Millions projected to be at risk from sea-level rise in the continental United States, *Na.e Clim. Change*, *6*(7), 691–695, doi:10.1038/nclimate2961.
Hemer, M. A., Y. Fan, N. Mori, A. Semedo, and X. L. Wang (2013), Projected changes in wave climate from a multi-model ensemble, *Nature Clim. Change*, *3*(5), 471–476, doi:10.1038/nclimate1791.
Hinkel, J., R. Nicholls, A. Vafeidis, R. J. Tol, and T. Avagianou (2010), Assessing risk of and adaptation to sea-level rise in the European Union: An application of DIVA, *Mitig. Adapt. Strateg. Glob. Change*, *15*(7), 703–719, doi:10.1007/s11027-010-9237-y.
Hinkel, J., D. Lincke, A. T. Vafeidis, M. Perrette, R. J. Nicholls, R. S. J. Tol, B. Marzeion, X. Fettweis, C. Ionescu, and A. Levermann (2014), Coastal flood damage and adaptation costs under 21st century sea-level rise, *Proc. Natl. Acad. Sci. U. S. A.*, *111*(9), 3292–3297, doi:10.1073/pnas.1222469111.
Howard, T., J. Lowe, and K. Horsburgh (2010), Interpreting century-scale changes in southern North Sea storm surge climate derived from coupled model simulations, *J. Clim.*, *23*(23), 6234–6247, doi:10.1175/2010jcli3520.1.
Howard, T., A. K. Pardaens, J. L. Bamber, J. Ridley, G. Spada, R. T. W. L. Hurkmans, J. A. Lowe, and D. Vaughan (2014), Sources of 21st century regional sea-level rise along the coast of northwest Europe, *Ocean Sci.*, *10*(3), 473–483, doi:10.5194/os-10-473-2014.
Intergovermental Panel on Climate Change (2013), Summary for policy makers, in *Climate Change 2013: The Physical Science Basis*, edited by T. F. Stocker, D. Qin, G.-K. Plattner, M. Tignor, S. K. Allen, J. Boschung, A. Nauels, Y. Xia, V. Bex, and P. M. Midgley , pp. 3–29 , Cambridge Univ. Press, Cambridge, U. K..
Intergovermental Panel on Climate Change (2014), Coastal systems and low-lying areas, in *IPCC WGII AR5*, Intergovermental Panel on Climate Change, Cambridge, U. K.
Jackson, L. P., and S. Jevrejeva (2016), A probabilistic approach to 21st century regional sea-level projections using RCP and High-end scenarios, *Global Planet. Change*, *146*, 179–189, doi:10.1016/j.gloplacha.2016.10.006.
Jagers, B., Rego J. L.; Verlaan, M.; Lalic, A.; Genseberger, M.; Friocourt, Y.; van der Pijl, S. (2014), A global tide and storm surge model with a parallel unstructured-grid shallow water solver, in *American Geophysical Union, Fall Meeting 2014*, San Francesco, Calif.
Jevrejeva, S., J. C. Moore, A. Grinsted, A. P. Matthews, and G. Spada (2014), Trends and acceleration in global and regional sea levels since 1807, *Global Planet. Change*, *113*, 11–22, doi:10.1016/j.gloplacha.2013.12.004.
Johansson, M. M., H. Pellikka, K. K. Kahma, and K. Ruosteenoja (2014), Global sea level rise scenarios adapted to the Finnish coast, *J. Mar. Syst.*, *129*, 35–46, doi:10.1016/j.jmarsys.2012.08.007.
Jordà, G., D. Gomis, E. Álvarez-Fanjul, and S. Somot (2012), Atmospheric contribution to Mediterranean and nearby Atlantic sea level variability under different climate change scenarios, *Global Planet. Change*, *80–81*, 198–214, doi:10.1016/j.gloplacha.2011.10.013.
Kendall, M. G. (1975), *Rank Correlation Methods*, Griffin, London, U. K..
Kopp, R. E., R. M. Horton, C. M. Little, J. X. Mitrovica, M. Oppenheimer, D. J. Rasmussen, B. H. Strauss, and C. Tebaldi (2014), Probabilistic 21st and 22nd century sea-level projections at a global network of tide-gauge sites, *Earth's Future*, *2*(8), 383–406, doi:10.1002/2014EF000239.
Little, C. M., R. M. Horton, R. E. Kopp, M. Oppenheimer, G. A. Vecchi, and G. Villarini (2015), Joint projections of US East Coast sea level and storm surge, *Nat. Clim. Change*, *5*(12), 1114–1120, doi:10.1038/nclimate2801.
Losada, I. J., B. G. Reguero, F. J. Méndez, S. Castanedo, A. J. Abascal, and R. Mínguez (2013), Long-term changes in sea-level components in Latin America and the Caribbean, *Global Planet. Change*, *104*, 34–50, doi:10.1016/j.gloplacha.2013.02.006.
Lowe, J. A., and J. M. Gregory (2005), The effects of climate change on storm surges around the United Kingdom, *Phil. Trans. R. Soc. A: Math. Phys. Eng. Sci.*, *363*(1831), 1313–1328, doi:10.1098/rsta.2005.1570.
Lowe, J. A., J. M. Gregory, and R. A. Flather (2001), Changes in the occurrence of storm surges around the United Kingdom under a future climate scenario using a dynamic storm surge model driven by the Hadley Centre climate models, *Clim. Dyn.*, *18*(3-4), 179–188, doi:10.1007/s003820100163.
Lowe, J. A., et al. (2009), UK Climate Projections science report: Marine and coastal projections, *Rep.*, Met Office Hadley Centre, Exeter, U. K.

Marcos, M., G. Jordà, D. Gomis, and B. Pérez (2011), Changes in storm surges in southern Europe from a regional model under climate change scenarios, *Global Planet. Change*, *77*(3–4), 116–128, doi:10.1016/j.gloplacha.2011.04.002.
Marcos, M., G. Chust, G. Jorda, and A. Caballero (2012), Effect of sea level extremes on the western Basque coast during the 21st century, *Clim. Res.*, *51*(3), 237–248, doi:10.3354/cr01069.
Marzeion, B., A. H. Jarosch, and M. Hofer (2012), Past and future sea-level change from the surface mass balance of glaciers, *Cryosphere*, *6*(6), 1295–1322, doi:10.5194/tc-6-1295-2012.
Matias, A., Ó. Ferreira, A. Vila-Concejo, T. Garcia, and J. A. Dias (2008), Classification of washover dynamics in barrier islands, *Geomorphology*, *97*(3–4), 655–674, doi:10.1016/j.geomorph.2007.09.010.
Mawdsley, R. J., I. D. Haigh, and N. C. Wells (2015), Global secular changes in different tidal high water, low water and range levels, *Earth's Future*, *3*(2), 66–81, doi:10.1002/2014EF000282.
McCall, R. T., J. S. M. Van Thiel de Vries, N. G. Plant, A. R. Van Dongeren, J. A. Roelvink, D. M. Thompson, and A. J. H. M. Reniers (2010), Two-dimensional time dependent hurricane overwash and erosion modeling at Santa Rosa Island, *Coast. Eng.*, *57*(7), 668–683, doi:10.1016/j.coastaleng.2010.02.006.
Mechler, R., L. M. Bouwer, J. Linnerooth-Bayer, S. Hochrainer-Stigler, J. C. J. H. Aerts, S. Surminski, and K. Williges (2014), Managing unnatural disaster risk from climate extremes, *Nat. Clim. Change*, *4*(4), 235–237, doi:10.1038/nclimate2137.
Meier, H. E. M. (2006), Baltic Sea climate in the late twenty-first century: A dynamical downscaling approach using two global models and two emission scenarios, *Clim. Dyn.*, *27*(1), 39–68, doi:10.1007/s00382-006-0124-x.
Meinshausen, M., et al. (2011), The RCP greenhouse gas concentrations and their extensions from 1765 to 2300, *Clim. Change*, *109*(1-2), 213–241, doi:10.1007/s10584-011-0156-z.
Mengel, M., A. Levermann, K. Frieler, A. Robinson, B. Marzeion, and R. Winkelmann (2016), Future sea level rise constrained by observations and long-term commitment, *Proc. Natl. Acad. Sci. U. S. A.*, *113*(10), 2597–2602, doi:10.1073/pnas.1500515113.
Mentaschi, L., G. Besio, F. Cassola, and A. Mazzino (2015), Performance evaluation of Wavewatch III in the Mediterranean Sea, *Ocean Model.*, *90*, 82–94, doi:10.1016/j.ocemod.2015.04.003.
Mentaschi, L., M. Vousdoukas, E. Voukouvalas, L. Sartini, L. Feyen, G. Besio, and L. Alfieri (2016), Non-stationary Extreme Value Analysis: A simplified approach for Earth science applications, *Hydrol. Earth Syst. Sci. Discuss.*, *2016*, 1–38, doi:10.5194/hess-2016-65.
Mentaschi, L., et al., (2017), Global variations of extreme coastal wave energy fluxes triggered by intensifying teleconnection patterns, *Geophys. Res. Lett.*, doi:10.1002/2016GL072488.
Mori, N., T. Shimura, T. Yasuda, and H. Mase (2013), Multi-model climate projections of ocean surface variables under different climate scenarios—Future change of waves, sea level and wind, *Ocean Eng.*, *71*, 122–129, doi:10.1016/j.oceaneng.2013.02.016.
Muis, S., M. Verlaan, H. C. Winsemius, J. C. J. H. Aerts, and P. J. Ward (2016), A global reanalysis of storm surges and extreme sea levels, *Nat. Commun.*, *7*, doi:10.1038/ncomms11969.
Oumeraci, H. (1994), Review and analysis of vertical breakwater failures—Lessons learned, *Coast. Eng.*, *22*(1–2), 3–29, doi:10.1016/0378-3839(94)90046-9.
Pardaens, A. K., J. A. Lowe, S. Brown, R. J. Nicholls, and D. de Gusmão (2011), Sea-level rise and impacts projections under a future scenario with large greenhouse gas emission reductions, *Geophys. Res. Lett.*, *38*(12), L12604, doi:10.1029/2011GL047678.
Pelling, H. E., and J. A. Mattias Green (2014), Impact of flood defences and sea-level rise on the European Shelf tidal regime, *Cont. Shelf Res.*, *85*, 96–105, doi:10.1016/j.csr.2014.04.011.
Peltier, W. R. (2004), Global glacial isostasy and the surface of the ice-age earth: The ICE-5G (VM2) model and GRACE, *Annu. Rev. Earth Planet. Sci.*, *32*, 111–149, doi:10.1146/annurev.earth.32.082503.144359.
Perez, J., M. Menendez, F. Mendez, and I. Losada (2014), Evaluating the performance of CMIP3 and CMIP5 global climate models over the north-east Atlantic region, *Clim. Dyn.*, *43*(9-10), 2663–2680, doi:10.1007/s00382-014-2078-8.
Perez, J., M. Menendez, P. Camus, F. J. Mendez, and I. J. Losada (2015), Statistical multi-model climate projections of surface ocean waves in Europe, *Ocean Model.*, *96*(Part 1), 161–170, doi:10.1016/j.ocemod.2015.06.001.
Pickering, M. D., N. C. Wells, K. J. Horsburgh, and J. A. M. Green (2012), The impact of future sea-level rise on the European Shelf tides, *Cont. Shelf Res.*, *35*, 1–15, doi:10.1016/j.csr.2011.11.011.
Queffeulou, P., and D. Croizé-Fillon (2014), Global altimeter SWH data set, *Rep.*, Laboratoire d'Océanographie Spatiale, IFREMER.
Rascle, N., and F. Ardhuin (2013), A global wave parameter database for geophysical applications. Part 2: Model validation with improved source term parameterization, *Ocean Model.*, *70*, 174–188, doi:10.1016/j.ocemod.2012.12.001.
Roland, A., Y. J. Zhang, H. V. Wang, Y. Meng, Y.-C. Teng, V. Maderich, I. Brovchenko, M. Dutour-Sikiric, and U. Zanke (2012), A fully coupled 3D wave-current interaction model on unstructured grids, *J. Geophys. Res. Oceans*, *117*(C11), doi:10.1029/2012JC007952.
Ruggiero, P. (2013), Is the intensifying wave climate of the U.S. Pacific Northwest increasing flooding and erosion risk faster than sea-level rise? *J. Waterw. Port Coast. Ocean Eng.*, *139*(2), 88–97, doi:10.1061/(asce)ww.1943-5460.0000172.
Sembiring, L., M. van Ormondt, A. van Dongeren, and D. Roelvink (2015), A validation of an operational wave and surge prediction system for the Dutch coast, *Nat. Hazards Earth Syst. Sci.*, *15*(6), 1231–1242, doi:10.5194/nhess-15-1231-2015.
Semedo, A., R. Weisse, A. Behrens, A. Sterl, L. Bengtsson, and H. Günther (2013), Projection of global wave climate change toward the end of the twenty-first century, *J. Clim.*, *26*(21), 8269–8288, doi:10.1175/jcli-d-12-00658.1.
Sierra, J. P., and M. Casas-Prat (2014), Analysis of potential impacts on coastal areas due to changes in wave conditions, *Clim. Change*, *124*(4), 861–876, doi:10.1007/s10584-014-1120-5.
Slangen, A. B. A., M. Carson, C. A. Katsman, R. S. W. van de Wal, A. Köhl, L. L. A. Vermeersen, and D. Stammer (2014), Projecting twenty-first century regional sea-level changes, *Clim. Change*, *124*(1), 317–332, doi:10.1007/s10584-014-1080-9.
Sterl, A., H. van den Brink, H. de Vries, R. Haarsma, and E. van Meijgaard (2009), An ensemble study of extreme storm surge related water levels in the North Sea in a changing climate, *Ocean Sci.*, *5*(3), 369–378, doi:10.5194/os-5-369-2009.
Tolman, H. L. (2002), *User manual and system documentation of WAVEWATCH-III version 2.22. Tech. report 222*, NOAA/NWS/NCEP/MMAB.
Tucker, M. J., and E. G. Pitt (2001), *Waves in Ocean Engineering* 521 pp., Elsevier, Amsterdam.
United Nations Framework Convention on Climate Change (2015), COP21 Paris agreement, [Available at http://unfccc.int/2860.php.]
United Nations Office for Disaster Risk Reduction (2015), Sendai framework for disaster risk reduction 2015–2030, *Rep.*, 37 pp., UNISDR, Geneva, Switzerland. [Available at http://www.unisdr.org/we/inform/publications/43291.]
U.S. Army Corps of Engineers (2002), *Coastal Engineering Manual*, U.S. Army Corps of Engineers, Washington, DC.
Vousdoukas, M. I., L. P. Almeida, and Ó. Ferreira (2012), Beach erosion and recovery during consecutive storms at a steep-sloping, meso-tidal beach, *Earth Surf. Process. Landforms*, *37*(6), 583–691, doi:10.1002/esp.2264.
Vousdoukas, M. I., E. Voukouvalas, A. Annunziato, A. Giardino, and L. Feyen (2016a), Projections of extreme storm surge levels along Europe, *Clim. Dyn.*, *47*(9), 3171–3190, doi:10.1007/s00382-016-3019-5.

Vousdoukas, M. I., E. Voukouvalas, L. Mentaschi, F. Dottori, A. Giardino, D. Bouziotas, A. Bianchi, P. Salamon, and L. Feyen (2016b), Developments in large-scale coastal flood hazard mapping, *Nat. Hazards Earth Syst. Sci.*, *16*, 1841–1853, doi:10.5194/nhess-16-1841-2016.

Wang, X. L., Y. Feng, and V. R. Swail (2014), Changes in global ocean wave heights as projected using multimodel CMIP5 simulations, *Geophys. Res. Lett.*, *41*(3), 1026–1034, doi:10.1002/2013GL058650.

Warner, J. C., B. Armstrong, R. He, and J. B. Zambon (2010), Development of a Coupled Ocean-Atmosphere-Wave-Sediment Transport (COAWST) modeling system, *Ocean Model.*, *35*(3), 230–244, doi:10.1016/j.ocemod.2010.07.010.

Weisse, R., H. von Storch, U. Callies, A. Chrastansky, F. Feser, I. Grabemann, H. Günther, J. Winterfeldt, K. Woth, and A. Pluess (2009), Regional meteorological-marine reanalyses and climate change projections: Results for Northern Europe and potential for coastal and offshore applications, *Bull. Am. Meteorol. Soc.*, *90*(6), 849–860, doi:10.1175/2008bams2713.1.

de Winter, R. C., A. Sterl, J. W. de Vries, S. L. Weber, and G. Ruessink (2012), The effect of climate change on extreme waves in front of the Dutch coast, *Ocean Dyn.*, *62*(8), 1139–1152, doi:10.1007/s10236-012-0551-7.

Woodworth, P. L. (2010), A survey of recent changes in the main components of the ocean tide, *Cont. Shelf Res.*, *30*(15), 1680–1691, doi:10.1016/j.csr.2010.07.002.

Woth, K., R. Weisse, and H. Von Storch (2006), Climate change and North Sea storm surge extremes: An ensemble study of storm surge extremes expected in a changed climate projected by four different regional climate models, *Ocean Dyn.*, *56*(1), 3–15, doi:10.1007/s10236-005-0024-3.

Zacharioudaki, A., S. Pan, D. Simmonds, V. Magar, and D. Reeve (2011), Future wave climate over the west-European shelf seas, *Ocean Dyn.*, *61*(6), 807–827, doi:10.1007/s10236-011-0395-6.

Zhang, K., Y. Li, H. Liu, J. Rhome, and C. Forbes (2013), Transition of the coastal and estuarine storm tide model to an operational storm surge forecast model: A case study of the Florida coast, *Weather Forecast.*, *28*(4), 1019–1037, doi:10.1175/waf-d-12-00076.1.

Zijl, F., M. Verlaan, and H. Gerritsen (2013), Improved water-level forecasting for the Northwest European Shelf and North Sea through direct modelling of tide, surge and non-linear interaction, *Ocean Dyn.*, *63*(7), 823–847, doi:10.1007/s10236-013-0624-2.